High-performance ternary organic solar cells with thick active layer exceeding 11% efficiency†

Nicola Gasparini,*[a] Luca Lucera,[b] Michael Salvador,[ac] Mario Prosa,[d] George D. Spyropoulos,[ae] Peter Kubis,[b] Hans-Joachim Egelhaaf,[b] Christoph J. Brabec[ae] and Tayebeh Ameri*[a]

We present a novel ternary organic solar cell with an uncommonly thick active layer (B300 nm), featuring thickness invariant charge carrier recombination and delivering 11% power conversion efficiency (PCE). A ternary blend was used to demonstrate photovoltaic modules of high technological relevance both on glass and flexible substrates, yielding 8.2% and 6.8% PCE, respectively.

The concept of organic bulk-heterojunction (BHJ) ternary solar cells has attracted increased interest in recent years for its capability to not only extend the spectral absorption range but also manipulate the recombination behavior of binary polymer: fullerene devices.[1–8] Typically consisting of two polymers (or small molecules) with complementary absorption spectra and one acceptor (or one donor and two acceptors), ternary blends surpassed the important 10% power conversion efficiency (PCE) threshold towards industrial application while maintaining the same level of simplicity for processing a single junction architecture.[4] The addition of a third absorber/chromophore is thus likely to contribute to a shorter energy payback time.[9]

Lately, a wide range of materials have been adopted to function as ternary sensitizers, such as polymers,[8,10–13] small molecules,[14] quantum dots[15] and dyes.[16,17] However, the charge transport limitations of many current generation polymer blends typically require rather low active layer thicknesses (around 100 nm) for optimum performance, limiting the internal quantum efficiency of thick active layers with more practical relevance (beyond 200 nm).

[a] *Institute of Materials for Electronics and Energy Technology (I-MEET), Friedrich-Alexander-University Erlangen-Nuremberg, Martensstraße 7, 91058 Erlangen, Germany. E-mail: nicola.gasparini@fau.de, tayebeh.ameri@fau.de*
[b] *ZAE Bayern – Solar Factory of the Future, Energy Campus Nurnberg, Furtherstrasse 250, 90429 Nurnberg, Germany*
[c] *Instituto de Telecomunicações, Instituto Superior Técnico, Av. Rovisco Pais, P-1049-001 Lisboa, Portugal*
[d] *Consiglio Nazionale delle Ricerche (CNR) – Istituto per lo Studio dei Materiali Nanostrutturati (ISMN), Via P. Gobetti, 101, 40129 Bologna, Italy*
[e] *Bavarian Center for Applied Energy Research (ZAE Bayern), Haberstrasse 2a, 91058 Erlangen, Germany*

Broader context

One key advantage of solution-processable organic semiconductors is the opportunity of blending different materials in order to attain novel material properties and applications. The concept of ternary blend organic solar cells makes use of exactly that idea: three (or more) organic chromphores are combined to better match the solar irradiance spectrum and thus increase the amount of light absorbed, which, in turn, will increase the power output of the solar cell. However, the charge transport limitations of many current generation polymer blends typically require rather low active layer thicknesses (around 100 nm) for optimum performance. Here, in addition to extending the absorption window of organic solar cells by adding a near infrared polymer, we demonstrate devices with unusually thick active layers (B300 nm) and power conversion efficiencies beyond 11%. Motivated by the possibility to process thick-film devices based on ternary blends, we demonstrate solar modules consisting of three solar cells connected is series, delivering 8.2% and 6.8% power conversion efficiency on glass and flexible substrates, respectively. These results underscore the relevance of ternary photovoltaic polymer blends for future upscaling technologies.

The reasons for the low performance are multiple. It could be associated with low charge carrier mobility because of reduced crystallinity.[18,19] In this case, the low purity of domains may translate into increased charge carrier recombination, leading to mainly poor fill factors (FF). A critical aspect affecting charge transport and the performance in general is the sensitive morphology of the active layer, which could have detrimental implications in the case of thick layers because of compositional gradients or strong variations in structural orientation.[18,19] Recently, important progress in PCEs has been achieved in the case of binary donor–acceptor thick film heterojunctions mainly due to the extensive research effort towards understandingand controlling the morphology of BHJ blends as well as the development of organic semiconductors with much improved charge transport capabilities.[19–21] While adding a third component to the bulk heterojunction may increase the spectral sensitivity of organic solar cell devices, it is apparent that it may also add complexity, making it difficult to uphold a morphology that maintains efficient transport, particularly

when envisioning solution processing *via* roll-to-roll coating using thick active layers.

In this communication, we report that the introduction of the near-infrared (NIR) absorbing polymer (poly[2,6-4,8-di(5-ethylhexylthienyl)benzo[1,2-*b*;3,3-*b*] dithiophene] [3-fluoro-2[(2-ethylhexyl)-carbonyl]thieno[3,4-*b*]thiophenediyl], (PTB7-th))[22] extends the absorption window of solar cells formed by relatively thick host films of PBTZT-stat-BDTT-8:$PC_{70}BM$[21] without adversely affecting the charge transport behavior. These devices are characterized by high internal quantum efficiencies (>90%) even for active layer thicknesses >300 nm. This strategy affords photovoltaic devices with optimized power conversion efficiency beyond 11% in the case of active layer thicknesses of >260 nm. We identify the occurrence of energy transfer followed by hole back transfer as the key mechanistic signature allowing for efficient device performance. Motivated by the possibility to process thick-film devices based on ternary blends, we demonstrate solar modules consisting of three solar cells connected in series, delivering 8.2% and 6.8% power conversion efficiency on glass and flexible substrates, respectively. These values highlight the up-scaling potential of ternary active layer devices as a valid alternative to the more complex multi-junction concept. Our findings inform that the formation of efficient ternary photovoltaic blends with practical relevance, *i.e.*, large active layer thicknesses, needs not to be limited to the polymers that perform exceptionally well in thick binary devices. Instead, the combination of energy transfer and hole back transfer in a ternary blend with complementary absorption signatures is a vital mechanism for extending the pool of promising material candidates for high performance organic solar cells with commercial significance.[23,24]

Most of the high efficiency polymer–fullerene ternary devices reported thus far have been processed in a conventional device architecture (low work function metal on top) with the potential drawback of poor device stability compared to the inverted architecture, which is more suitable for upscaling applications.[24,25] For this reason, we fabricated organic BHJ ternary solar cells using an inverted device layout based on indium tin oxide (ITO)/ZnO/active layer/MoOx/Ag (see the ESI† and Fig. S1 for the materials used and the device layout). In order to explore the highest performances, we varied the amount of the NIR sensitizer (Table S1 in the ESI†) while the overall polymer to fullerene ratio was kept constant at 1 : 1.5 by weight. Table 1 summarizes the photovoltaic parameters for the best ternary and corresponding binary BHJ solar cells.

The reason for choosing PTB7-th as the ternary sensitizer is twofold: the possibility of extending the spectral coverage beyond the absorption of PBTZT-STAT-BDTT-8 (Fig. 1a) and its ability to deliver a similar open circuit voltage (V_{oc}) to PBTZT-STAT-BDTT-8:$PC_{70}BM$ binary devices due to the almost identical HOMO energies of the polymers (Fig. 3). Fig. 1b shows the representative current density *vs.* voltage (*J*–*V*) characteristics of the control devices and ternary systems under simulated AM 1.5G solar irradiation (100 mW cm^{-2}). Both PBTZT-STAT-BDTT-8:$PC_{70}BM$ and PTB7-th:$PC_{70}BM$ reference blends delivered power conversion efficiencies of >8.6%, which is in line with the current state-of-the-art for these polymer solar cells.[6,21] As expected, the incorporation of 50% of PTB7-th into the host PBTZT-STAT-BDTT-8:$PC_{70}BM$ did not alter the V_{oc} of ternary organic devices compared to the corresponding binary solar cells (0.77 V). On the other hand, the ternary devices yielded an enhanced PCE of 10.2% owing to an increase in the short circuit current (J_{sc}) of 11% and 15% compared to PBTZT-STAT-BDTT-8:$PC_{70}BM$ and PTB7-th:$PC_{70}BM$ binary devices, respectively, and a high fill factor (FF) of 71%. Such high fill factors are not uncommon in ternary composites and are often the result of a strongly suppressed recombination behavior.[12] As a result, we obtained an average PCE of 10.06% for 18 devices (Fig. S2, ESI†). Notably, the optimum power conversion efficiency was achieved for an active layer thickness of 260 nm, considerably higher compared to the state-of-the-art thickness of PTB7-th based devices, which is usually >110 nm.[22] The PCE of the ternary devices can be further enhanced to values beyond 11% when reducing the active area, mainly because of an improved fill factor (Table 1). In this case, the champion device yielded a J_{sc} of 19.35 mA cm^{-2}, a V_{oc} of 0.77 V and an FF of 74%, resulting in a power conversion efficiency of 11.03% (Fig. S3, ESI†).

We performed external quantum efficiency measurements (EQE) to elucidate the different contributions to the photon-to-current conversion and to confirm the current density values obtained from the current–voltage traces. Fig. 1a and Fig. S4 (ESI†) show an extended spectral response of ternary devices compared to the host PBTZT-STAT-BDTT-8-based binary system while maintaining a similar maximum EQE of 75%. In contrast to PTB7-th based binary devices, ternary solar cells feature reduced optical interference, which we associate with the increased active layer thickness with which the ternary blends were processed.

As reported by Berny *et al.*,[21] PBTZT-STAT-BDTT-8-based binary polymer–fullerene blends maintain high efficiency up

Table 1 Photovoltaic device parameters of single solar cells and modules on plastic and glass substrates prepared in this work

PBTZT-STAT-BDTT-8 : PTB7-th : $PC_{70}BM$	Area [mm^2]	V_{oc} [V]	J_{sc} [mA cm^{-2}]	FF [%]	PCE [%]
1 : 0 : 1.5	10.4	0.78 (0.78 0.01)	16.68 (16.39 0.19)	67.08 (66.70 0.28)	8.64 (8.16 0.44)
0.5 : 0.5 : 1.5	10.4	0.77 (0.77 0.01)	18.67 (18.53 0.08)	71.07 (70.58 0.76)	10.21 (10.06 0.14)
0.5 : 0.5 : 1.5	2	0.77 (0.77 0.01)	19.35 (19.17 0.15)	74.05 (73.59 0.77)	11.03 (10.61 0.35)
0 : 1 : 1.5	10.4	0.77 (0.77 0.01)	15.92 (15.57 0.28)	69.13 (68.47 0.47)	8.66 (8.33 0.20)
0.5 : 0.5 : 1.5 on IMI	10.4	0.75 (0.75 0.02)	15.2 (14.93 0.24)	69 (68.85 0.32)	7.87 (7.48 0.38)
0.5 : 0.5 : 1.5 module on glass/ITO	10.4	2.3 (2.30 0.02)	5.38[a] (5.20 0.15)	66 (64.72 1.28)	8.16 (7.89 0.27)
0.5 : 0.5 : 1.5 module on IMI	10.4	2.2 (2.20 0.03)	5.01[a] (4.53 0.38)	62 (60.63 1.37)	6.83 (6.48 0.30)

[a] Current density calculated over the total area.

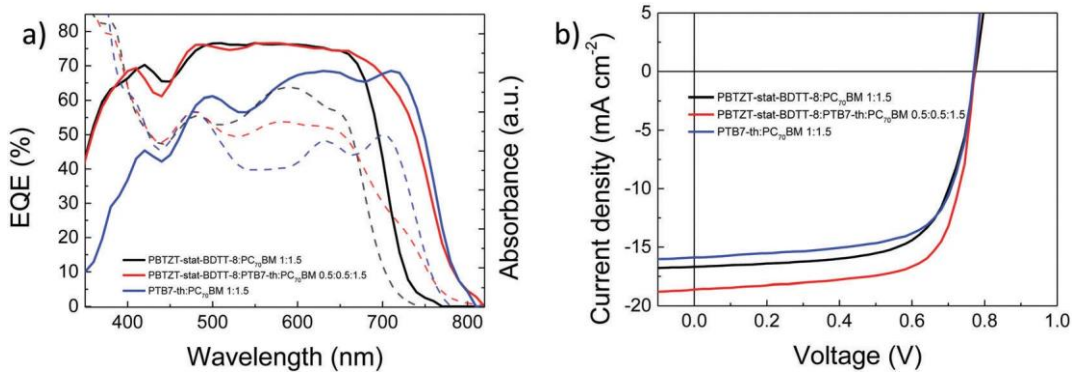

Fig. 1 (a) Absorption profiles (dotted lines) and spectrally resolved external quantum efficiency (solid lines) of the binary and ternary bulk-heterojunction solar cells studied in this work. (b) Current-voltage characteristics of PBTZT-STAT-BDTT-8:$PC_{70}BM$, PBTZT-STAT-BDTT-8:PTB7-th:$PC_{70}BM$ and PTB7-th:$PC_{70}BM$ based solar cells probed under 100 mW cm^{-2} simulated solar irradiance.

to active layer thicknesses of ß500 nm. We therefore studied the influence of the thickness on the photovoltaic performance and charge transport behavior of ternary blends based on PBTZT-STAT-BDTT-8 and PTB7-th. This is important because PTB7-th based devices are known to be highly sensitive to active layer thickness variations.[19] Fig. 2a compares the PCE as a function of the active layer thickness for the ternary and the corresponding binary solar cells. Significantly, for ternary active layers, the PCE exceeds 9% over the thickness range of 150 to 330 nm. A similar trend, but with lower efficiency, is also observed for PBTZT-STAT-BDTT-8-based binary devices, as reported earlier.[21] In contrast, the efficiency of PTB7-th solar cells decreases dramatically when processed into devices with active layer thicknesses beyond 100 nm, in agreement with previous reports.[26,27]

Fig. 2b depicts the FF values as a function of active layer thickness for ternary as well as binary blends. Notably, for the same active layer thickness range of 150–330 nm fill factors between 65% and 74% and 65–70% are extracted from the *J*–*V* characteristics of PBTZT-STAT-BDTT-8:PTB7-th:$PC_{70}BM$ and PBTZT-STAT-BDTT-8:$PC_{70}BM$ based devices, respectively. Furthermore, analysis of the photovoltaic parameters allows concluding that the dramatic drop in the PCE of PTB7-th-based devices (Fig. 2a) is primarily linked to the steep decrease in FF values (see also Fig. S2, ESI†).

In order to shed light on the transport behavior of ternary devices, we investigated the charge carrier mobility m of finished devices by employing the technique of photoinduced charge carrier extraction by linearly increasing voltage (photo-CELIV) (Fig. S5, ESI†).[28–30] Photo-CELIV measurements allow the faster charge carrier mobility to be calculated directly from a solar cell without the realization of hole-only and/or electron only stacks.[31,32] The center graph of Fig. 2b displays the calculated mobility as a function of the active layer thickness for ternary and binary blends. Crucially, the charge carrier mobility of the ternary blends is not significantly affected by thickness variations and achieves a maximum value of 9.8×10^{-4} cm^2 V^{-1} s^{-1} (260 nm), corresponding to a 11% and 72% improvement compared to the highest mobility for PBTZT-STAT-BDTT-8:$PC_{70}BM$ (290 nm) and PTB7-th:$PC_{70}BM$ (100 nm) based binary systems, respectively. The rather constant carrier mobility is likely one of the reasons for the invariance of the FF and the overall efficiency with respect to the active layer thickness. Similarly, the charge carrier mobility for the PBTZT-STAT-BDTT-8-based binary devices varies only gently with increasing blend thickness. Conversely, PTB7-th based binary blends suffer a reduction in charge carrier mobility of almost 1 order of magnitude

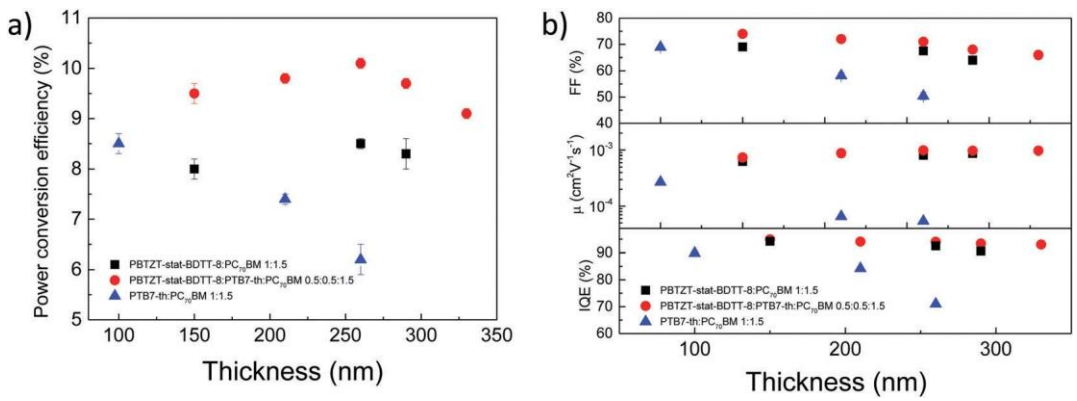

Fig. 2 (a) Power conversion efficiency of binary and ternary devices as a function of active layer thickness. (b) Fill factor (top), charge carrier mobility (middle) and integrated IQE (bottom) as a function of the active layer thickness of PBTZT-STAT-BDTT-8:$PC_{70}BM$, PBTZT-STAT-BDTT-8:PTB7-th: $PC_{70}BM$ and PTB7-th:$PC_{70}BM$ based devices.

(5.4×10^{-5} cm^2 V^{-1} s^{-1} at 260 nm active layer thickness) compared to the optimum active layer thickness. These results confirm the charge transport limitations of the PTB7 based polymer family.[19] On the other hand, a carrier mobility and FF that are rather insensitive to the thickness of the active layer should afford an internal quantum efficiency close to 100%.[33,34] We calculated the internal quantum efficiency (IQE) of PBTZT-STAT-BDTT-8:PTB7-th:$PC_{70}BM$ solar cells using a systematic approach reported elsewhere (Fig. S6, ESI†).[35,36] As shown in the bottom graph of Fig. 2b the IQE values exceed 92% throughout 150 to 330 nm active layer thicknesses, indicating that this system is not affected by recombination losses.[33,37,38] A similar IQE *vs.* thickness behavior is found for PBTZT-STAT-BDTT-8:$PC_{70}BM$, while in the case of PTB7-th:$PC_{70}BM$ we observe a rapid decay of the IQE with increasing active layer thickness, consistent with the loss in FF and reduced charge carrier mobility for this system. The thickness dependent charge transport measurements further inform that the ternary blend is unlikely to suffer from microstructure limitations of the blended polymers. In fact, both topography and phase signals from intermittent contact mode atomic force microscopy (AFM) measurements (Fig. S8, ESI†), although predominantly surface sensitive,[39] reveal that the introduction of PTB7-th in the PBTZT-STAT-BDTT-8:PC70BM binary blend does not induce notable changes in topography, implying high compatibility between the two donor polymers. The latter is corroborated by the efficient fluorescence quenching, as shown in Fig. 3a and discussed below. Furthermore, the improved J_{sc} and FF in the case of the ternary blend support the argument of high structural compatibility. We emphasize that correlating the bulk microstructure with optoelectronic device performance is generally challenging and beyond the scope of thecurrent work.

The photovoltaic performance and charge carrier mobility data presented thus far suggest that the thickness-resistant charge transport behavior of the ternary blends is mainly related to the transport characteristics of the polymer PBTZT- STAT-BDTT-8. This is surprising given that PTB7-th constitutes 50% of the donor blend in the ternary composite. In order to further elucidate the charge transport mechanism of the tern- ary system, we performed photoluminescence (PL) and carrier selective current–voltage measurements.

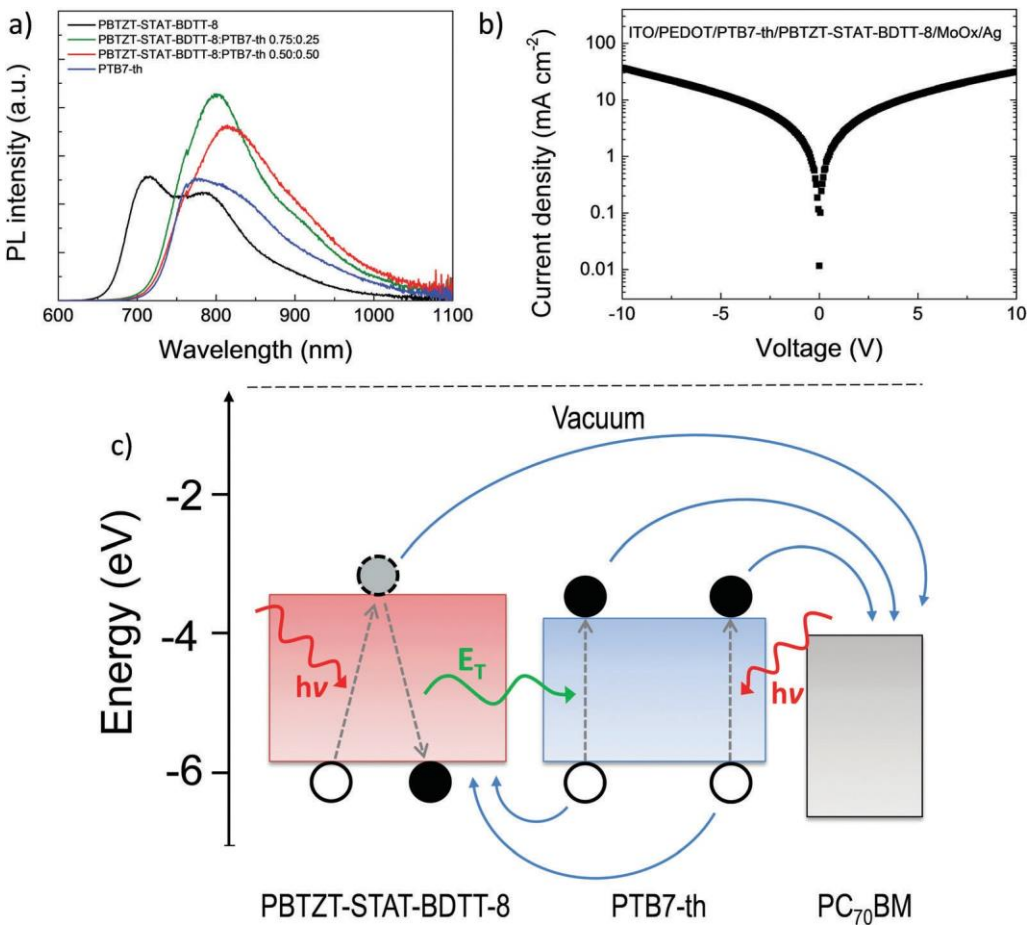

Fig. 3 (a) Photoluminescence (PL) spectra of pure PBTZT-STAT-BDTT-8 and PTB7-th polymers and different PBTZT-STAT-BDTT-8:PTB7-th blend ratios. All PL spectra are normalized by taking into account the optical density of each film. (b) Current-density characteristics of the hole-only bilayer device. (c) Schematic of the charge and energy transfer (E_T) mechanisms involved in the ternary blend. Hollow spheres represent holes, while filled spheres represent electrons. The energy of the frontier orbitals reflect values reproduced from the literature.[6,21]

Fig. 3a provides a quantitative comparison of the photo-luminescence (PL) spectra of the pure PBTZT-STAT-BDTT-8 and PTB7-th polymers with the PL of the PBTZT-STAT-BDTT-8: PTB7-th binary blend under 405 nm laser light excitation (see the ESI† for details). PBTZT-STAT-BDTT-8 depicts two distinct peaks at 710 and 790 nm, whereas PTB7-th features one broad peak centred at 795 nm. Importantly, the higher energy fluores-cence peak of PBTZT-STAT-BDTT-8 is effectively quenched when blended with the low band gap polymer PTB7-th, regard-less of the ratio of the two polymers. Concomitantly, the emission of PTB7-th is enhanced as compared to the pristine PTB7-th film, suggesting energy transfer from PBTZT-STAT- BDTT-8 to PTB7-th. (Fig. 3c)[11,40,41] We note that the occurrence of non-radiative Förster resonance energy transfer (FRET) has been proposed as a relevant process for improving the perfor- mance of ternary blends.[5,40,41] An effective FRET requires over- lap between the absorption band of one component (acceptor) and the emission band of the other component (donor). In fact, the absorption band of PTB7-th overlaps with the emission band of PBTZT-STAT-BDTT-8 to the extent that energy transferfrom the wide to the low bang gap polymer is likely to occur, as shown in Fig. S5 (ESI†). However, our charge carrier mobility study strongly suggests that it is the PBTZT-STAT-BDTT-8 matrix that mainly dominates charge transport. This can be rationalized, if we assume that efficient charge (hole) back transfer occurs from the HOMO of PTB7-th to the HOMO of PBTZT-STAT-BDTT-8 upon photoexcitation of PTB7-th. To testour hypothesis, we fabricated hole-only bilayer devices of PTB7-th and PBTZT-STAT-BDTT-8 (Fig. 3b).[6] This approach has proven particularly useful for disentangling electronic drivingforces in ternary blends.[6] In this case, the *J–V* curve appears
highly symmetric from +10 to —10 V. This means that holes can be easily transferred between the two polymers, in agreement with the energy diagram shown in Fig. 3c, which infers a small energy difference between the HOMO levels of the two polymers. Given that the charge carrier mobility is larger in the case of PBTZT-STAT-BDTT-8, it is feasible that charge carriers once transferred remain in the PBTZT-STAT-BDTT-8 phase prior to being extracted, instead of transferring back to the PTB7-th phase. Overall, we conclude that because of the equal amounts of PBTZT-STAT-BDTT-8 and PTB7-th present in the optimum ternary blend, it is plausible that energy transfer among these two polymers is upheld even in the presence of fullerene. However, while this mechanism may favor the splitting of excitons located further away from the donor–acceptor interface, we suggest that it is the charge transfer mechanism *via* the HOMOs of the polymers that is responsible for the improved opto-electronic response of the ternary blend.

Motivated by the ease of device fabrication and high efficiency of the PBTZT-STAT-BDTT-8:PTB7-th:$PC_{70}BM$ ternary blend we thus asked whether this material system is suitable for delivering efficient power output when implemented in a photovoltaic module, and possibly for mitigating the commonly observed efficiency gap between lab devices and modules.[23,24,42] Photo-voltaic modules represent an important test bed because real-world applications typically require large voltage outputs, which can be achieved through monolithic interconnection of consecutive cells.[43,44] We thus prepared solar modules follow-ing a procedure outlined by Spyropoulos *et al.*[45] The process involves high precision, ultrafast laser structuring of sequen-tial, uniformly coated layers to form interconnects with low series resistance and reduced dead area. We chose glass/ITO and PET/ITO-Ag-ITO (IMI)[42] substrates to realize both rigid and flexible devices, respectively. In order to achieve functional modules, three laser steps are necessary: the P1 laser defines the bottom electrode, the P2 line ‘‘opens’’ the photoactive layerto create a contact between the top and bottom electrode and P3 electrically separates the top electrode (Fig. 4a and Table S3, ESI†). More details on the monolithic interconnection of organic solar modules can be found elsewhere.[24] The area between the P1 and the P3 line is not photo-active and thus can be considered a loss region (dead area). This gives rise to the geometric fill factor (GFF), which is defined as $\mathrm{GFF} = 1 - \frac{\text{Dead area}}{\text{Total area}}$ %.

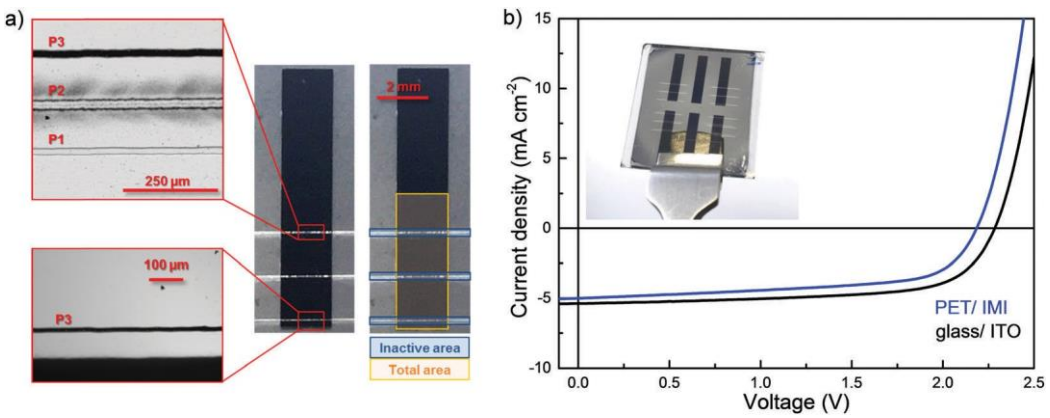

Fig. 4 (a) Optical micrographs of a solar module with three interconnected sub-cells. The insets on the left represent optical magnifications of the interconnection region, where the laser lines P1, P2 and P3 are highlighted. The photo-inactive (dead area, blue) and total area (yellow) of the module are highlighted as well. (b) Light *J–V* curves of flexible and rigid modules prepared using the ternary blend PBTZT-STAT-BDTT-8 : PTB7-th : $PC_{70}BM$ (0.5 : 0.5 : 1.5) as the photoactive layer. The inset shows a photograph of a glass/ITO substrate including 4 modules and 2 reference cells (center).

The closer the GFF is to 100%, the lower the impact of the patterning technique on the final PCE of the solar module. In this work, laser structuring allowed us to achieve interconnection regions of 250–300 mm and thus GFFs as high as 90%.

Fig. 4 displays the optical micrographs and photographs of the solar modules as well as the light *J*–*V* characteristics. A summary of the photovoltaic parameters of the reference single cells and modules is provided in Table 1. We achieved solar module efficiencies as high as 8.16% on glass and 6.83% on flexible substrates, which are among the highest values reported to date.[46,47] When compared with solar cells, the PCE of solar modules is mainly limited by the lower short-circuit current, which can be attributed to a reduced active area of the modules (GFF E 90%) and lower transparency of the IMI electrode compared to ITO.[42] Flexible modules achieved 87% of the PCE of the reference flexible solar cell and modules on glass 80% of the performance of the record solar cell. Additional sources of losses are commonly related to the resistance of the interconnecting area, for instance, due to laser patterning debris, as previously reported.[24] Improving upon the individual cell's active areas can lead to higher GFF values and is one rational strategy to alleviate module-specific losses. We emphasize that despite these initial performance gaps, our demonstrations highlight the potential of ternary organic semiconductor based single junction devices as a simple yet efficient alternative to multi-junction solar modules.

In conclusion, we report a novel high performance photovoltaic system based on an organic ternary blend that delivers a power conversion efficiency beyond 11%. We elucidate that the combination of the two polymers PBTZT-STAT-BDTT-8 and PTB7-th in the photoactive layer not only offers the possibility of better matching the solar irradiance spectrum but also allows the fabrication of solar cells featuring active layer thicknesses much beyond what is commonly considered as the optimum for PTB7-th based photovoltaics. Charge transport and IQE measurements reveal that the recombination behavior in PBTZT-STAT-BDTT-8:PTB7-th:$PC_{70}BM$ devices is nearly thickness-insensitive for photoactive layers up to B350 nm. We explain this observation with effective hole transfer from PTB7-th to PBTZT-STAT-BDTT-8, which may occur upon direct excitation of PTB7-th or upon energy transfer from PBTZT-STAT-BDTT-8 to PTB7-th. In this system, PTB7-th thus acts predominantly as an NIR sensitizer, a concept that could be exploited for NIR sensitive photodetectors. Conversely, the thickness-insensitive performance of the PBTZT-STAT-BDTT-8:PTB7-th:$PC_{70}BM$ ternary blend makes it particularly suitable for upscaling purposes, where a robust, thick active layer helps prevent shunting problems induced by roll-to-roll coating.[21,48] The demonstration of photovoltaic modules with state of the art performance underscores the technological relevance of ternary organic solar cells for practical applications with large voltage requirements. Overall, these results may provide a strategy to reevaluate high performance polymers that are typically limited to B100 nm active layer thicknesses and motivate the use of ternary blends as a valid alternative to the more complex multi-junction devices.

Experimental section

Fabrication of photovoltaic device and measurements

Pre-structured indium tin oxide (ITO) substrates were cleaned with acetone and isopropyl alcohol in an ultrasonic bath for 10 minutes each. After drying, the substrates were coated with 40 nm of zinc oxide (ZnO) and B100 nm thick active layer based on PBTZT-STAT-BDTT-8:PTB7-th:$PC_{70}BM$ (25 g L^{-1} in a mixture of chlorobenzene (CB) and 1,8-diiodooctane 97 to 3 vol%). To complete the fabrication of the devices, 10 nm of MoOx and 100 nm of Ag were thermally evaporated through a mask (with a 10.4 mm^2 active area opening) under a vacuum of B1 $\times$ 10^{-6} mbar. The *J*–*V* characteristics were measured using a source measurement unit from BoTest. Illumination was provided by a solar simulator (Oriel Sol 1A, from Newport) with AM1.5G light at 100 mW cm^{-2}. UV-VIS absorption was performed on a Lambda 950, from Perkin Elmer. EQEs were measured using an integrated system from Enlitech, Taiwan. All the devices were tested in ambient air.

Photo-CELIV

In photo-CELIV measurements, the devices were illuminated with a 405 nm laser-diode. Current transients were recorded across an internal 50 O resistor of an oscilloscope (Agilent Technologies DSO-X 2024A). We used a fast electrical switch to isolate the cell and prevent charge extraction or sweep out during the laser pulse and the delay time. After a variable delay time, a linear extraction ramp is applied *via* a function generator. The ramp, which was 60 ms long and 2 V in amplitude, was set to start with an offset matching the V_{oc} of the cell for each delay time. From the measured photocurrent transients, the charge carrier mobility (m) is calculated using the followingeqn (1):

$$m = \frac{2d^2}{3At_{max}^2\left(1 + 0.36\frac{\Delta j}{j(0)}\right)} \quad \text{if} \quad \Delta j \le j0; \qquad (1)$$

where d is the active layer thickness, A is the voltage rise speed $A = dU/dt$, U is the applied voltage, t_{max} is the time corresponding to the maximum of the extraction peak, and $j(0)$ is the displacement current.

Photoluminescence

Photoluminescence measurements were performed on active layers, which were excited with a 405 nm laser. The PL emission of the films was dispersed by a 600 lines per mm grating monochromator (HRS-2) and detected by an Indium Gallium Arsenide (InGaAs) detector (ADC 403L) through a lock-in technique. The fluorescence spectrum was corrected for the optical density of the sample at the excitation wavelength, and for the detection sensitivity of the InGaAs detector.

AFM

AFM measurements were performed on a solver nano from NT-MDT using 300 kHz single crystal silicon cantilevers (Nt-MDT, NSG30).

Acknowledgements

This project has received funding from the European Community's Seventh Framework Programme (FP7/2007-2013) under the Grant Agreement no. 607585 project OSNIRO. M. S. acknowledges primary support from a fellowship by the Portuguese Fundação *para* a Ciência e a Tecnologia (SFRH/BPD/71816/2010). The authors gratefully acknowledge the support of the Cluster of Excellence ''Engineering of Advanced Materials'' at the University of Erlangen-Nuremberg, which is funded by the German Research Foundation (DFG) within the framework of its ''Excellence Initiative'', Synthetic Carbon Allotropes (SFB953) and Solar Technologies go Hybrid (SolTech).

References

1 L. Lu, M. A. Kelly, W. You and L. Yu, *Nat. Photonics*, 2015, 9, 491–500.

2 Q. An, F. Zhang, J. Zhang, W. Tang, Z. Deng and B. Hu, *Energy Environ. Sci.*, 2016, 9, 281–322.

3 T. Ameri, P. Khoram, J. Min and C. J. Brabec, *Adv. Mater.*, 2013, 25, 4245–4266.

4 L. Nian, K. Gao, F. Liu, Y. Kan, X. Jiang, L. Liu, Z. Xie, X. Peng, T. P. Russell and Y. Ma, *Adv. Mater.*, 2016, 28, 8184–8190.

5 T. Goh, J.-S. Huang, K. G. Yager, M. Y. Sfeir, C.-Y. Nam, X. Tong, L. M. Guard, P. R. Melvin, F. Antonio, B. G. Bartolome, M. L. Lee, N. Hazari and A. D. Taylor, *Adv. Energy Mater.*, 2016, 6, 1600660.

6 N. Gasparini, X. Jiao, T. Heumueller, D. Baran, G. J. Matt, S. Fladischer, E. Spiecker, H. Ade, C. J. Brabec and T. Ameri, *Nat. Energy*, 2016, 1, 16118.

7 M. Prosa, M. Tessarolo, M. Bolognesi, T. Cramer, Z. Chen, A. Facchetti, B. Fraboni, M. Seri, G. Ruani and M. Muccini, *Adv. Mater. Interfaces*, 2016, 3, 1600770.

8 T. Kumari, S. M. Lee, S. Kang, S. Chen and C. Yang, *Energy Environ. Sci.*, 2017, 10, 258–265.

9 S. B. Darling and F. You, *RSC Adv.*, 2013, 3, 17633–17648.

10 T. Ameri, J. Min, N. Li, F. Machui, D. Baran, M. Forster, K. J. Schottler, D. Dolfen, U. Scherf and C. J. Brabec, *Adv. Energy Mater.*, 2012, 2, 1198–1202.

11 N. Gasparini, M. Salvador, S. Fladischer, A. Katsouras, A. Avgeropoulos, E. Spiecker, C. L. Chochos, C. J. Brabec and T. Ameri, *Adv. Energy Mater.*, 2015, 5, 1501527.

12 Y. (Michael) Yang, W. Chen, L. Dou, W. Chang, H. Duan, B. Bob, G. Li and Y. Yang, *Nat. Photonics*, 2015, 9, 190–198.

13 L. Lu, T. Xu, W. Chen, E. S. Landry and L. Yu, *Nat. Photonics*, 2014, 8, 716–722.

14 J. Zhang, Y. Zhang, J. Fang, K. Lu, Z. Wang, W. Ma and Z. Wei, *J. Am. Chem. Soc.*, 2015, 137, 8176–8183.

15 G. Itskos, A. Othonos, T. Rauch, S. F. Tedde, O. Hayden, M. V. Kovalenko, W. Heiss and S. a. Choulis, *Adv. Energy Mater.*, 2011, 1, 802–812.

16 L. Ke, J. Min, M. Adam, N. Gasparini, Y. Hou, J. D. Perea, W. Chen, H. Zhang, S. Fladischer, A.-C. Sale, E. Spiecker, R. R. Tykwinski, C. J. Brabec and T. Ameri, *Adv. Energy Mater.*, 2016, 6, 1502355.

17 W. Keawsongsaeng, J. Gasiorowski, P. Denk, K. Oppelt, D. H. Apaydin, R. Rojanathanes, K. Hingerl, M. Scharber, N. S. Sariciftci and P. Thamyongkit, *Adv. Energy Mater.*, 2016, 1600957.

18 B. A. Collins, Z. Li, J. R. Tumbleston, E. Gann, C. R. Mcneill and H. Ade, *Adv. Energy Mater.*, 2013, 3, 65–74.

19 Y. Liu, J. Zhao, Z. Li, C. Mu, W. Ma, H. Hu, K. Jiang, H. Lin, H. Ade and H. Yan, *Nat. Commun.*, 2014, 5, 5293.

20 V. Vohra, K. Kawashima, T. Kakara, T. Koganezawa, I. Osaka, K. Takimiya and H. Murata, *Nat. Photonics*, 2015, 9, 403–408.

21 S. Berny, N. Blouin, A. Distler, H.-J. Egelhaaf, M. Krompiec, A. Lohr, O. R. Lozman, G. E. Morse, L. Nanson, A. Pron, T. Sauermann, N. Seidler, S. Tierney, P. Tiwana, M. Wagner and H. Wilson, *Adv. Sci.*, 2016, 3, 1500342.

22 Z. He, B. Xiao, F. Liu, H. Wu, Y. Yang, S. Xiao, C. Wang, T. P. Russell and Y. Cao, *Nat. Photonics*, 2015, 9, 174–179.

23 L. Lucera, F. Machui, P. Kubis, H. D. Schmidt, J. Adams, S. Strohm, T. Ahmad, K. Forberich, H.-J. Egelhaaf and C. J. Brabec, *Energy Environ. Sci.*, 2015, 9, 89–94.

24 L. Lucera, P. Kubis, F. W. Fecher, C. Bronnbauer, M. Turbiez, K. Forberich, T. Ameri, H.-J. Egelhaaf and C. J. Brabec, *Energy Technol.*, 2015, 3, 373–384.

25 M. Prosa, M. Tessarolo, M. Bolognesi, O. Margeat, D. Gedefaw, M. Gaceur, C. Videlot-Ackermann, M. R. Andersson, M. Muccini, M. Seri and J. Ackermann, *ACS Appl. Mater. Interfaces*, 2016, 8, 1635–1643.

26 A. Calabrese, G. Schimperna, R. Po, T. Yohannes, S. E. Debebe, F. Tinti and N. Camaioni, *J. Appl. Phys.*, 2011, 110, 113106.

27 H. W. Ro, J. M. Downing, S. Engmann, A. A. Herzing, D. M. DeLongchamp, L. J. Richter, S. Mukherjee, H. Ade, M. Abdelsamie, L. K. Jagadamma, A. Amassian, Y. Liu and H. Yan, *Energy Environ. Sci.*, 2016, 9, 2835–2846.

28 A. Pivrikas, N. S. Sariciftci, G. Juška and R. Österbacka, *Prog. Photovoltaics*, 2007, 15, 677–696.

29 N. Gasparini, A. Katsouras, M. I. Prodromidis, A. Avgeropoulos, D. Baran, M. Salvador, S. Fladischer, E. Spiecker, C. L. Chochos, T. Ameri and C. J. Brabec, *Adv. Funct. Mater.*, 2015, 25, 4898–4907.

30 T. M. Clarke, C. Lungenschmied, J. Peet, N. Drolet and A. J. Mozer, *Adv. Energy Mater.*, 2015, 5, 1401345.

31 A. Armin, G. Juska, M. Ullah, M. Velusamy, P. L. Burn, P. Meredith and A. Pivrikas, *Adv. Energy Mater.*, 2014, 4, 1300954.

32 V. Mihailetchi, J. Wildeman and P. Blom, *Phys. Rev. Lett.*, 2005, 94, 126602.

33 D. U. Karatay, M. Salvador, K. Yao, A. K.-Y. Jen and D. S. Ginger, *Appl. Phys. Lett.*, 2014, 105, 33304.

34 S. H. Park, A. Roy, S. Beaupre, S. Cho, N. Coates, J. S. Moon, D. Moses, M. Leclerc, K. Lee and A. J. Heeger, *Nat. Photonics*, 2009, 3, 297–303.

35 C. O. Ramírez Quiroz, I. Levchuk, C. Bronnbauer, M. Salvador, K. Forberich, T. Heumüller, Y. Hou, P. Schweizer, E. Spiecker and C. J. Brabec, *J. Mater. Chem. A*, 2015, 3, 24071–24081.

36 G. F. Burkhard, E. T. Hoke and M. D. McGehee, *Adv. Mater.*, 2010, 22, 3293–3297.

37 P. Peumans, V. Bulović and S. R. Forrest, *Appl. Phys. Lett.*, 2000, 76, 2650.

38 S. Albrecht, S. Schäfer, I. Lange, S. Yilmaz, I. Dumsch, S. Allard, U. Scherf, A. Hertwig and D. Neher, *Org. Electron.*, 2012, 13, 615–622.

39 W. Chen, M. P. Nikiforov and S. B. Darling, *Energy Environ. Sci.*, 2012, 5, 8045.

40 L. Lu, W. Chen, T. Xu and L. Yu, *Nat. Commun.*, 2015, 6, 7327.

41 V. Gupta, V. Bharti, M. Kumar, S. Chand and A. J. Heeger, *Adv. Mater.*, 2015, 27, 4398–4404.

42 P. Kubis, L. Lucera, F. Machui, G. Spyropoulos, J. Cordero, A. Frey, J. Kaschta, M. M. Voigt, G. J. Matt, E. Zeira and C. J. Brabec, *Org. Electron.*, 2014, 15, 2256–2263.

43 F. C. Krebs, N. Espinosa, M. Hösel, R. R. Søndergaard and M. Jørgensen, *Adv. Mater.*, 2014, 26, 29–39.

44 R. R. Søndergaard, M. Hösel and F. C. Krebs, *J. Polym. Sci., Part B: Polym. Phys.*, 2013, 51, 16–34.

45 G. D. Spyropoulos, P. Kubis, N. Li, D. Baran, L. Lucera, M. Salvador, T. Ameri, M. M. Voigt, F. C. Krebs and C. J. Brabec, *Energy Environ. Sci.*, 2014, 7, 3284–3290.

46 S. Hong, H. Kang, G. Kim, S. Lee, S. Kim, J.-H. Lee, J. Lee, M. Yi, J. Kim, H. Back, J.-R. Kim and K. Lee, *Nat. Commun.*, 2016, 7, 1–6.

47 M. A. Green, K. Emery, Y. Hishikawa, W. Warta and E. D. Dunlop, *Prog. Photovoltaics*, 2016, 24, 905–913.

48 G. D. Spyropoulos, C. O. Ramirez Quiroz, M. Salvador, Y. Hou, N. Gasparini, P. Schweizer, J. Adams, P. Kubis, N. Li, E. Spiecker, T. Ameri, H. Egelhaaf and C. J. Brabec, *Energy Environ. Sci.*, 2016, 9, 2302–2313.